Ultrafast Ising Machines using spin torque nano-oscillators

Dagur Ingi Albertsson, Mohammad Zahedinejad, Afshin Houshang, et al.

View Online   Export Citation   CrossMark

ARTICLES YOU MAY BE INTERESTED IN

Ultrafast Ising Machines using spin torque nano-oscillators

Dagur Ingi Albertsson,[1] (iD) Mohammad Zahedinejad,[2,3] (iD) Afshin Houshang,[2,3] (iD) Roman Khymyn,[2] (iD)
Johan Åkerman,[2,3,a)] (iD) and Ana Rusu[1,a)] (iD)

AFFILIATIONS

[1]Division of Electronics and Embedded Systems, KTH Royal Institute of Technology, 164 40 Kista, Sweden
[2]Physics Department, University of Gothenburg, 412 96 Gothenburg, Sweden
[3]NanOsc AB, Electrum 229, 164 40 Kista, Sweden

[a)]Authors to whom correspondence should be addressed: johan.akerman@physics.gu.se and arusu@kth.se

ABSTRACT

Combinatorial optimization problems are known for being particularly hard to solve on traditional von Neumann architectures. This has led to the development of Ising Machines (IMs) based on quantum annealers and optical and electronic oscillators, demonstrating speed-ups compared to central processing unit (CPU) and graphics processing unit (GPU) algorithms. Spin torque nano-oscillators (STNOs) have shown GHz operating frequency, nanoscale size, and nanosecond turn-on time, which would allow their use in ultrafast oscillator-based IMs. Here, we show using numerical simulations based on STNO auto-oscillator theory that STNOs exhibit fundamental characteristics needed to realize IMs, including in-phase/out-of-phase synchronization and second harmonic injection locking phase binarization. Furthermore, we demonstrate numerically that large STNO network IMs can solve Max-Cut problems on nanosecond timescales.

Combinatorial optimization (CO) problems appear in a wide range of scheduling, routing, and optimization situations in all of society. CO problems can be illustrated as the need for finding a global minimum in a multivariate energy landscape. As this is a very common situation in nature, solutions have been inspired by physical systems such as the Ising model.[1] The Hamiltonian associated with the Ising model can be written as

$$H = -\sum_{j,j'}^{N} J_{j,j'} s_j s_{j'} - h \sum_{j}^{N} s_j, \qquad (1)$$

where N represents the number of spins, $J_{j,j'}$ is the coupling between spins j and j', s_j is the spin state $+1$ or -1 of spin j, and the last term describes a bias field h acting on all spins. Real-world CO problems can be mapped[1] onto the Hamiltonian in Eq. (1), which opens up the possibility of building a general purpose CO computing platform based on solving the Ising model.

Customized hardware architectures able to solve the Ising model Eq. (1) are called Ising Machines (IMs), and various implementations have been proposed. D-Wave quantum annealers based on Josephson junctions[2] have shown promising results but face similar challenges as general quantum computers: cryogenic temperatures requiring kWs of cooling power and extremely high production costs. IMs utilizing optoelectronic parametric oscillators address some challenges related to quantum systems, offering room temperature operation and all-to-all interconnections using optical feedback methods.[3–5] However, solutions to miniaturize these systems are challenging and are yet to be demonstrated. Alternatively, IMs inspired by simulated annealing and based on commercially available CMOS processes have shown promising results.[6–8]

A recent demonstration using LC oscillators and resistive crossbars proved that IM can be realized utilizing readily available electronic oscillators.[9,10] This approach is based on the similarities between the Ising Hamiltonian and the Lyapunov function describing the dynamics of a second harmonic injection locked (SHIL) network of coupled oscillators.

Networks of synchronized spintronic oscillators such as spin-torque nano-oscillators (STNOs) and spin-Hall nano-oscillators (SHNOs),[11] with characteristics including wide frequency tunability, nanoscale size, strongly non-linear behavior, and CMOS compatibility, have gained significant interest as building blocks for neuromorphic/unconventional computing.[12–19] These properties, along with the substantial effort focused on further enhancing the controllability of spintronic oscillator arrays,[20,21] make them interesting candidates for

implementing IMs. It is, therefore, of great interest to explore whether networks of interacting STNOs, with their particularly strong and qualitatively different non-linearities, could be used as IMs. Here, we numerically explore this possibility.

The proposed IM consists of an array of coupled STNOs where SHIL is achieved by applying a small RF current, with twice the frequency of the free-running STNOs, in combination with the DC bias current to all the STNOs. To predict the behavior of such a network, we employ the universal auto-oscillator model proposed by Slavin and Tiberkevich,[22] which describes the STNO dynamics in terms of the complex dimensionless spin wave amplitude c, where $p = |c^2|$ is proportional to the STNO output power and $\phi = arg(c)$ is the phase. The dynamical equations describing STNO j in an array under SHIL can be written as[22,23]

$$\frac{dc_j}{dt} + i\omega_j(p_j)c_j + \Gamma_{+,j}(p_j)c_j - \Gamma_{-,j}(p_j)c_j$$
$$= K_e e^{-i\omega_e t}c_j^* + \sum_{j'} \Omega_{j,j'} e^{i\beta_{j,j'}} c_{j'} \qquad (2)$$

or alternatively as two coupled real differential equations for the power p and phase ϕ as

$$\frac{dp_j}{dt} = -2p_j\left[\Gamma_{+,j}(p_j) - \Gamma_{-,j}(p_j)\right] + 2K_e p_j \cos(\omega_e t + 2\phi_j)$$
$$+ 2\sum_{j,j'} \Omega_{j,j'} \sqrt{p_j p_{j'}} \cos(\phi_j - \phi_{j'} - \beta_{j,j'}), \qquad (3a)$$

$$\frac{d\phi_j}{dt} = -\omega_j(p_j) - K_e \sin(\omega_e t + 2\phi_j)$$
$$+ \sum_{j,j'} \Omega_{j,j'} \sqrt{p_{j'}/p_j} \sin(\phi_{j'} - \phi_j + \beta_{j,j'}), \qquad (3b)$$

where $\omega_j(p_j) = \omega_0 + \mathcal{N}p_j$ is the operating frequency, $\omega_0/2\pi \approx 4.2\,GHz$ is the ferromagnetic resonance frequency, $\mathcal{N}/2\pi \approx -3.44\,GHz$ is the nonlinear frequency shift coefficient, $\Gamma_{+,j}(p_j) = \Gamma_G(1 + Qp_j)$ is the intrinsic magnetization damping ($\Gamma_G/2\pi \approx 252\,MHz$), and $Q \approx 2.66$ is the nonlinear damping parameter. $\Gamma_{-,j}(p_j) = \sigma I_{dc}(1 - p_j)$ is the negative damping induced by the spin polarized direct current I_{dc} and $\sigma = \varepsilon g\mu_B/2eM_sV$, where $\varepsilon = 0.7$ is the spin polarization, g is the spectroscopic Lande factor, μ_B is the Bohr magneton, e is the electron charge, $4\pi M_s = 9500\,Oe$ is the saturation magnetization, and $V = 85 \times 140 \times 1.8\ nm^3$ is the volume of the free layer. Parameters, including $\mathcal{N}$ and ω_0, were calculated based on a CoFeB magnetic tunnel junction STNO,[24] as shown in Fig. 1(a), with an easy-plane magnetic anisotropy of $H_A = 125\,Oe$ and placed in an external in-plane magnetic field of $H_{ext} = 300\,Oe$ oriented at an angle of $\phi_{ext} = 30°$ with respect to the anisotropy direction of the free layer. Moreover, the inter-layer coupling field is assumed as $H_{int} = 125\,Oe$. All device parameters are taken from an analytical model developed in Ref. 25, which was successfully used to replicate the microwave signal properties of different independent magnetic tunnel junction STNO studies.[24,26]

Injection locking is described using the frequency ω_e of the external RF current and its coupling strength, K_e to the STNOs. The last term on the right-hand side (RHS) describes the coupling of oscillator j to other oscillators j' in the network through the coupling strength $\Omega_{j,j'}$ and phase $\beta_{j,j'}$. Common coupling mechanisms between STNOs include spin-wave,[12–15,27,28] direct exchange,[16,19,29] dipolar,[30–32] and electrical[18,33–35] coupling, or even a combination of these mechanisms.[12,15,18,19] However, the type of coupling does not directly affect the model in Eq. (2) where only the strength and phase of the coupling mechanism are taken into account. Throughout the simulation results, we will focus on the behavior of the STNO system described by Eq. (2) without explicitly defining the type of coupling. However, a general
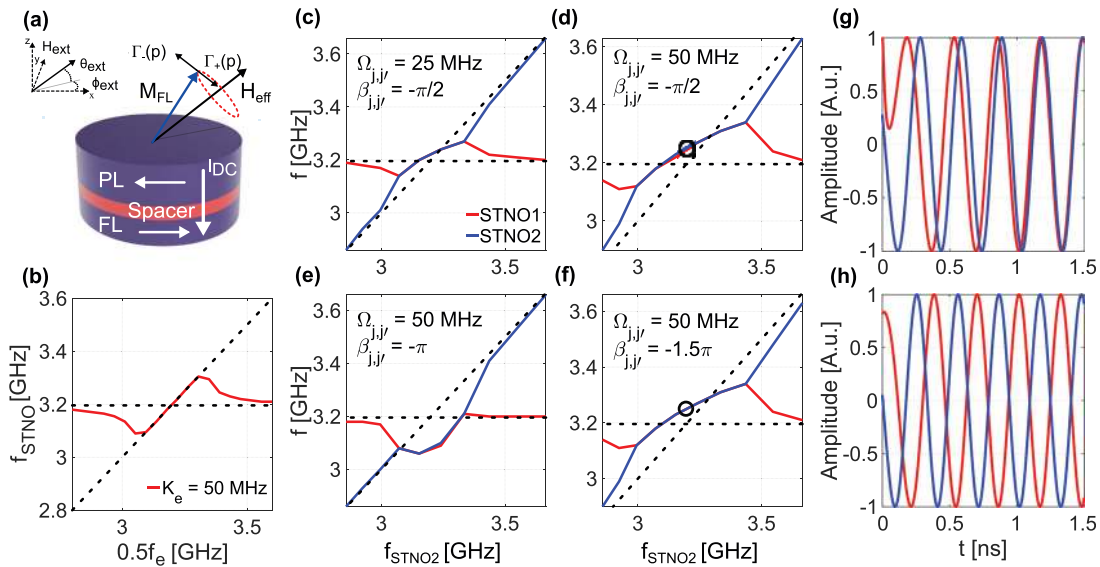
FIG. 1. (a) STNO and graphical representation of terms in Eq. (2). PL is the pinned layer, FL is the free layer, M_{FL} is the magnetization of the free layer, and H_{eff} is the effective field inside the FL; (b) SHIL of a single STNO; Simulations of two coupled STNOs: (c), (d), (e), and (f) show mutual synchronization of the two STNOs for different coupling strength and phases; (g) and (h) show the transients of the STNOs corresponding to the black circular mark in (d) and (f).

purpose IM requires an all-to-all coupling, which limits the choice of physical coupling mechanisms.

Figure 1(b) presents simulation results for a single injection locked STNO [the last term on the RHS in Eq. (2) is neglected], where ω_e is swept around the STNO second harmonic, the so-called second harmonic injection locking (SHIL), with a fixed value of coupling to the external RF current, $K_e = 50$ MHz. For a large difference between $f_e = \omega_e/2\pi$ and f_{STNO}, the STNO remains at the free running frequency of 3.2 GHz. However, when f_e approaches $2f_{STNO}$, it starts perturbing the STNO, showing a typical frequency pulling between 2.9 GHz and 3.1 GHz, while the STNO completely locks to the external signal in the range of 3.1 GHz - 3.3 GHz. Similar to conventional electronic oscillators under SHIL, there are two stable locking states with a relative phase difference of 180°. This behavior is often referred to as phase binarization, which is critical for the realization of an oscillator-based IM. In the case of a single locked oscillator, the locking states 0°/180° depend purely on the initial conditions. However, for a network of coupled oscillators under SHIL, these two states can be used to represent spins in the Ising Hamiltonian as it has been previously demonstrated.[9]

Figures 1(c)–1(h) present the simulation results obtained by solving Eq. (2) for two identical coupled STNOs in the absence of SHIL [$K_e = 0$ in Eq. (2)]. STNO$_1$ is biased with a constant DC bias current resulting in $f_{STNO_1} \approx 3.2$ GHz, while the DC bias/operating frequency of STNO$_2$ is swept. Figures 1(c) and 1(d) present the effect of increasing $\Omega_{j,j'}$, which results in a wider frequency locking range. Moreover, the STNOs synchronize away from the mean of their individual operating frequencies as a consequence of the coupling phase $\beta_{j,j'}$.[22,35]

The coupling phase characterizes the phase delay associated with the coupling mechanism, e.g., in the case of dipolar coupling $\beta_{j,j'} = -\pi/2$.[22] Moreover, the coupling phase can be re-normalized to account for any other time delays of the coupling, such as, e.g., capacitive coupling.[36–38] A change in $\beta_{j,j'}$ significantly modifies the locking bandwidth and the frequency at which the STNOs synchronize, as presented in Figure 1(d) and 1(e). Moreover, for the case of $\beta_{j,j'} = -1.5\pi$ shown in Fig. 1(f), the STNOs synchronize in frequency but are out-of-phase (OOP) as presented in Fig. 1(h). This translates to a negative (antiferromagnetic) coupling $\Omega_{j,j'}$ in Eq. (2). For the conventional electronic oscillator, the OOP synchronization usually occurs in

the fixed range of $0.5\pi < \beta_{j,j'} < 1.5\pi$, while the nonlinearity in STNOs shifts this interval when Eq. (2) is solved.[39] Analytically, the effective coupling phase, $\tilde{\beta}_{j,j'}$, can be approximated as[22]

$$\tilde{\beta}_{j,j'} = \beta_{j,j'} - \tan^{-1}(\nu), \tag{4}$$

where ν is the normalized nonlinear frequency shift coefficient, calculated according to the macrospin theory.[22] For the case presented in Fig. 1(h), $\nu \approx -2.64$, which translates to an effective coupling phase of $\tilde{\beta}_{j,j'} \approx -1.1\pi$, explaining why a robust OOP synchronization is achieved under these conditions. The combination of in-phase/OOP synchronization and SHIL phase binarization demonstrated above shows that STNOs exhibit all the desired characteristics to realize an IM.

Many NP-hard problems can be mapped onto the Ising model, but we will focus on a particular class of problems called Max-Cut, one of Karp's 21 NP-complete problems. Specifically, we focus on undirected, unweighted graphs with N vertices and E edges. The Max-Cut problem consists of partitioning the vertices into two subsets s_1/s_2 such that the number of edges crossing between s_1 and s_2 is as high as possible. This problem can be mapped to the Hamiltonian in Eq. (1) (assuming $h = 0$) where spins that settle to the states $\uparrow$ / $\downarrow$ (+1/−1) belong to the subset s_1/s_2. An optimal solution of a particular graph corresponds to the sets s_1/s_2 leading to the ground state of Eq. (1), which also represents the Max-Cut solution. An example graph, called a Möbius ladder graph with a size $N = 16$, is shown in Fig. 2(a) along with one possible ground state/Max-Cut solution.

In the oscillator-based IM, STNOs represent nodes/spins with the state +1/-1 determined by the phase 0°/180° and with graph edges programed into the couplings $\Omega_{j,j'}$. Max-Cut problems require antiferromagnetic coupling $\Omega_{j,j'}$ between STNOs if nodes in a particular graph are connected and $\Omega_{j,j'} = 0$ otherwise. The coupling phase is chosen as $\beta_{j,j'} = -1.4\pi$ to yield an effective coupling phase of $\tilde{\beta}_{j,j'} \approx -\pi$, which provides antiferromagnetic coupling in our simulations. Moreover, we assume that the STNOs are biased with $I_{dc} = 1.5$ mA, leading to $\omega_j(p)/2\pi \approx 3.2$ GHz with a coupling strength of $\Omega_{j,j'} = 25$ MHz (if nodes are connected) and $\omega_e/2\pi = 2 \times 3.2$ GHz for SHIL.

It has been shown that employing SHIL for annealing in LC oscillator-based IM can increase the probability of achieving the
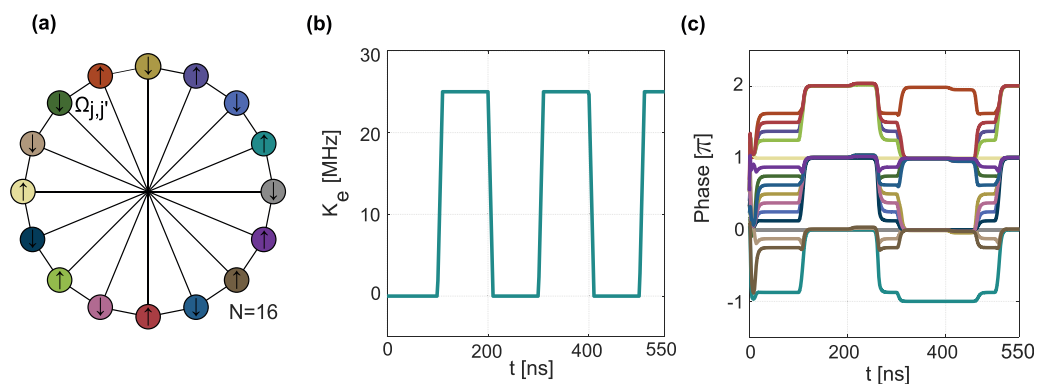
FIG. 2. (a) Möbius ladder graph of size $N = 16$ and one possible ground state where nodes with 0°/180° ($\uparrow$ / $\downarrow$) states belong to the subset s_1/s_2. (b) Annealing is performed by ramping K_e repeatedly as a function of time. (c) Evolution of the phase difference between STNOs connected as in (a) when $\Omega_{j,j'} = 25$ MHz, $\beta_{j,j'} = -1.4\pi$, and K_e follows the annealing schedule in (b).

optimal solution.[9] STNOs exhibit qualitatively different characteristics compared to conventional electronic oscillators, which can be seen from Eq. (3) where the phase ϕ and power p are strongly coupled. Moreover, SHIL in STNOs strongly influences p, which consequently affects the coupling in the network through $\sqrt{p_{j'}/p_j}\Omega_{j,j'}$. To explore the effect of SHIL on the STNO-based IM, we employ the annealing schedule shown in Fig. 2(b).

It is worth mentioning that K_e is proportional to the amplitude of the injected RF current at ω_e and consequently, implementing such an annealing schedule in experiments should be relatively straightforward. This annealing schedule was chosen arbitrarily and does not guarantee optimal performance, but comparison of annealing schedules or finding an optimal annealing schedule is out of the scope of this study.

The phase difference between STNOs employing the previously presented annealing schedule is shown in Fig. 2(c). During the first 100 ns, the STNOs distribute relatively uniformly from -π to π as a consequence of the phase coupling $\beta_{j,j'}$. The state they reach within these 100 ns is already close to the optimal solution, provided that one reassigns their individual continuous phase values to the closest 0°/180° phase state. At $t = 100$ ns, K_e is ramped from 0 to 25 MHz over 10 ns to phase binarize the network, which forces the STNOs to settle to a phase close to 0° or 180°. This process is then repeatedly performed to search for the global optimal/Max-Cut solution. While this small network finds its solution already during the first such step, larger networks require many annealing steps to find their minimum. Every time the SHIL is switched off, there is a substantial delay before the STNOs return to their intrinsic phase state. This delay is longer for stronger SHIL and is a consequence of the sum term in Eq. (3b), which is very close to zero in the SHIL state; the stronger the SHIL, the closer to zero those terms will be.

We then explored the impact of different sizes of Möbius ladder graphs using the annealing schedule in Fig. 2(b). In Fig. 3(a), the probability of achieving the optimal solution in 100 simulation runs with and without SHIL as a function of Möbius ladder graph size is presented. The phases ϕ of all STNOs are initialized with a random uniform distribution between $[0, 2\pi]$, while the initial power p is kept as 0.3, which is close to the free running STNO power. In the case without SHIL, the final phase difference is rounded to the nearest multiple

of π to extract the cut value. Figure 3(a) confirms that SHIL improves the Max-Cut probability in the proposed STNO-based IM. Additionally, in Fig. 3(b), a comparison between the achieved cut as a function of time with and without annealing for a single run for $N = 288$ is shown. For both cases, the network quickly reaches a solution close to the Max-Cut (within the first 100 ns), but SHIL perturbs the STNO array, leading to a Max-Cut solution, while without SHIL, the system is stuck, close to the Max-Cut. To further confirm this conclusion, the inset in Fig. 3(b) shows the probability distribution of cuts for $N = 288$ over 100 runs. Without SHIL, solutions close to the Max-Cut exhibit the highest probability, while SHIL modifies the distribution, increasing the Max-Cut probability.

We have verified the functionality of the STNO-based IM and shown that SHIL significantly increases the solution quality. However, Möbius ladder graphs are classified as "easy" Max-Cut problems.[40] To further demonstrate the potential of the proposed architecture, we employ random cubic (3-regular) graphs which can be considered as "hard" Max-Cut problems.[40] An example graph of size N = 16 is shown in Fig. 4(a). We generate 20 random graphs of each size, ranging from 16 to 256, and again employ the annealing schedule shown in Fig. 2(b). The Max-Cut solutions are determined using LocalSolver, a commercially available optimization tool, and compared with the solution found by the STNO IM. The results are presented in Fig. 4(b) where each data point represents the average probability of 20 random graphs in 100 runs (total of 2000 simulations). The error bars represent one standard deviation of the probability, which indicates the distribution of hardness for different graphs of the same size. As expected, the probability of finding the Max-Cut solution for random graphs is significantly lower than that for the Möbius graphs, confirming the hardness of these problems. Fig. 4(b) also presents the probability of finding a sub-optimal solution, which is less than 5 cuts from the Max-Cut solution.

It is noteworthy that in all our simulations, we never observed any chaotic behavior, which has been shown to arise in coupled STNOs under certain conditions, in particular, as the number of STNOs increases.[39,41] It was also shown that it may even be beneficial for STNO-based reservoir computing to operate at the edge of chaos.[42] While it is beyond the scope of our work to address the impact of possible chaos, which could possibly appear in much larger STNO networks, it is something that future studies should investigate.
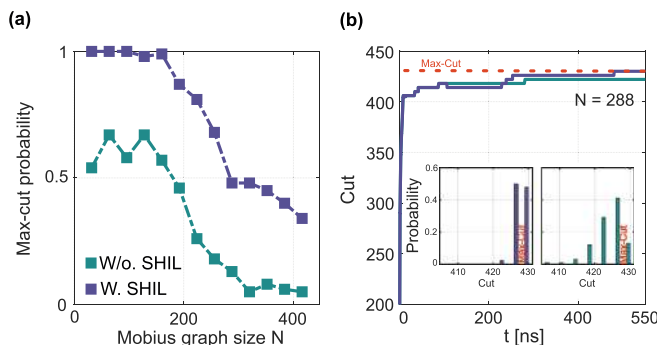

FIG. 3. (a) Probability of achieving the Max-Cut solution for Möbius ladder graphs of different sizes and (b) the achieved cut as a function of annealing time for a single run of N = 288 with and without SHIL. The inset in (b) shows the cut probability distribution with and without SHIL from 100 runs.
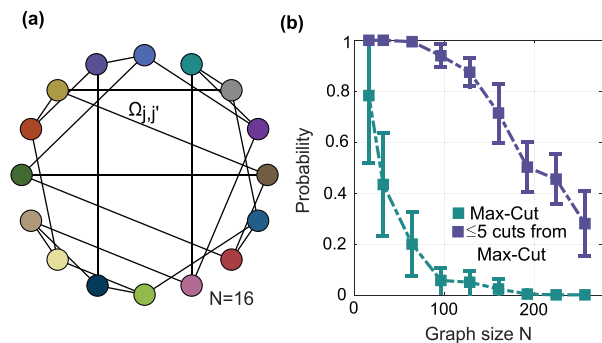

FIG. 4. (a) Random cubic graph of size N = 16 and (b) the mean probability of obtaining the Max-Cut solution (green) and a sub-optimal solution (purple) for 20 different random cubic graphs of each size.

We have shown that STNOs exhibit fundamental characteristics required to develop an ultrafast and nanoscale IM. However, to achieve an experimental demonstration of a spintronic oscillator-based IM, further research on synchronization of large STNO/SHNO networks is required. Specifically, a general purpose IM requires an all-to-all coupling, which is impossible to achieve using, e.g., dipolar coupling alone. One potential solution might be to employ dipolar/exchange or spinwave coupling for physically close STNOs, while electrical coupling could be used for longer distances. Additionally, an efficient method to control the coupling strength and even the coupling phase needs to be developed to demonstrate a general purpose IM. From a fundamental perspective, the impact of phase noise, variability, and graph density needs to be further explored to fully understand the potential of the proposed spintronic oscillator IM.

DATA AVAILABILITY

The data that support the findings of this study are available from the corresponding author upon reasonable request.

REFERENCES

[1]A. Lucas, "Ising formulations of many NP problems," Front. Phys. **2**, 1–14 (2014).

[2]M. W. Johnson, M. H. Amin, S. Gildert, T. Lanting, F. Hamze, N. Dickson, R. Harris, A. J. Berkley, J. Johansson, P. Bunyk, E. M. Chapple, C. Enderud, J. P. Hilton, K. Karimi, E. Ladizinsky, N. Ladizinsky, T. Oh, I. Perminov, C. Rich, M. C. Thom, E. Tolkacheva, C. J. Truncik, S. Uchaikin, J. Wang, B. Wilson, and G. Rose, "Quantum annealing with manufactured spins," Nature **473**, 194–198 (2011).

[3]T. Inagaki, Y. Haribara, K. Igarashi, T. Sonobe, S. Tamate, T. Honjo, A. Marandi, P. L. McMahon, T. Umeki, K. Enbutsu, O. Tadanaga, H. Takenouchi, K. Aihara, K. I. Kawarabayashi, K. Inoue, S. Utsunomiya, and H. Takesue, "A coherent Ising machine for 2000-node optimization problems," Science **354**, 603–606 (2016).

[4]P. McMahon, A. Marandi, Y. Haribara, R. Hamerly, C. Langrock, S. Tamate, T. Inagaki, H. Takesue, S. Utsunomiya, K. Aihara, R. L. Byer, M. M. Fejer, H. Mabuchi, and Y. Yamamoto, "A fully programmable 100-spin coherent Ising machine with all-to-all connections," Science **354**, 614 (2016).

[5]R. Hamerly, T. Inagaki, P. L. McMahon, D. Venturelli, A. Marandi, T. Onodera, E. Ng, C. Langrock, K. Inaba, T. Honjo, K. Enbutsu, T. Umeki, R. Kasahara, S. Utsunomiya, S. Kako, K. I. Kawarabayashi, R. L. Byer, M. M. Fejer, H. Mabuchi, D. Englund, E. Rieffel, H. Takesue, and Y. Yamamoto, "Experimental investigation of performance differences between coherent Ising machines and a quantum annealer," Sci. Adv. **5**, eaau0823 (2019).

[6]M. Yamaoka, C. Yoshimura, M. Hayashi, T. Okuyama, H. Aoki, and H. Mizuno, "A 20k-spin Ising chip to solve combinatorial optimization problems with CMOS annealing," IEEE J. Solid-State Circuits **51**, 303–309 (2016).

[7]T. Takemoto, M. Hayashi, C. Yoshimura, and M. Yamaoka, "A 2 x 30k-spin multi-chip scalable cmos annealing processor based on a processing-in-memory approach for solving large-scale combinatorial optimization problems," IEEE J. Solid-State Circuits **55**, 145–156 (2020).

[8]K. Yamamoto, K. Ando, N. Mertig, T. Takemoto, M. Yamaoka, H. Teramoto, A. Sakai, S. Takamaeda-Yamazaki, and M. Motomura, "STATICA: A 512-spin 0.25M-weight full-digital annealing processor with a near-memory all-spin-updates-at-once architecture for combinatorial optimization with complete spin-spin interactions," in IEEE International Solid-State Circuits Conference, Digest of Technical Papers (2020), pp. 138–140.

[9]T. Wang and J. Roychowdhury, "Oim: Oscillator-based ising machines for solving combinatorial optimisation problems," in *Unconventional Computation and Natural Computation*, edited by I. McQuillan and S. Seki (Springer International Publishing, Cham, 2019), pp. 232–256.

[10]J. Chou, S. Bramhavar, S. Ghosh, and W. Herzog, "Analog coupled oscillator based weighted Ising machine," Sci. Rep. **9**, 1–10 (2019).

[11]T. Chen, R. K. Dumas, A. Eklund, P. K. Muduli, A. Houshang, A. A. Awad, P. Dürrenfeld, B. G. Malm, A. Rusu, and J. Akerman, "Spin-torque and spin-hall nano-oscillators," Proc. IEEE **104**, 1919–1945 (2016), 1512.03162.

[12]S. Kaka, M. R. Pufall, W. H. Rippard, T. J. Silva, S. E. Russek, and J. A. Katine, "Mutual phase-locking of microwave spin torque nano-oscillators," Nature **437**, 389–392 (2005).

[13]F. B. Mancoff, N. D. Rizzo, B. N. Engel, and S. Tehrani, "Phase-locking in double-point-contact spin-transfer devices," Nature **437**, 393–395 (2005).

[14]S. Sani, J. Persson, S. M. Mohseni, Y. Pogoryelov, P. K. Muduli, A. Eklund, G. Malm, M. Käll, A. Dmitriev, and J. Akerman, "Mutually synchronized bottom-up multi-nanocontact spin-torque oscillators," Nat. Commun. **4**, 2731 (2013).

[15]A. Houshang, E. Iacocca, P. Dürrenfeld, S. R. Sani, J. Akerman, and R. K. Dumas, "Spin-wave-beam driven synchronization of nanocontact spin-torque oscillators," Nat. Nanotechnol. **11**, 280–286 (2016).

[16]A. A. Awad, P. Dürrenfeld, A. Houshang, M. Dvornik, E. Iacocca, R. K. Dumas, and J. Åkerman, "Long-range mutual synchronization of spin Hall nano-oscillators," Nat. Phys. **13**, 292–299 (2017).

[17]J. Torrejon, M. Riou, F. A. Araujo, S. Tsunegi, G. Khalsa, D. Querlioz, P. Bortolotti, V. Cros, K. Yakushiji, A. Fukushima, H. Kubota, S. Yuasa, M. D. Stiles, and J. Grollier, "Neuromorphic computing with nanoscale spintronic oscillators," Nature **547**, 428–431 (2017), 1701.07715.

[18]M. Romera, P. Talatchian, S. Tsunegi, F. Abreu Araujo, V. Cros, P. Bortolotti, J. Trastoy, K. Yakushiji, A. Fukushima, H. Kubota, S. Yuasa, M. Ernoult, D. Vodenicarevic, T. Hirtzlin, N. Locatelli, D. Querlioz, and J. Grollier, "Vowel recognition with four coupled spin-torque nano-oscillators," Nature **563**, 230–234 (2018), 1711.02704.

[19]M. Zahedinejad, A. A. Awad, S. Muralidhar, R. Khymyn, H. Fulara, H. Mazraati, M. Dvornik, and J. Åkerman, "Two-dimensional mutually synchronized spin Hall nano-oscillator arrays for neuromorphic computing," Nat. Nanotechnol. **15**, 47–52 (2020).

[20]H. Fulara, M. Zahedinejad, R. Khymyn, M. Dvornik, S. Fukami, S. Kanai, H. Ohno, and J. Åkerman, "Giant voltage-controlled modulation of spin Hall nano-oscillator damping," Nat. Commun. **11**, 1–7 (2020).

[21]M. Zahedinejad, H. Fulara, R. Khymyn, A. Houshang, S. Fukami, S. Kanai, H. Ohno, and J. Åkerman, "Memristive control of mutual SHNO synchronization for neuromorphic computing," arXiv:2009.06594 (2020).

[22]A. Slavin and V. Tiberkevich, "Nonlinear auto-oscillator theory of microwave generation by spin-polarized current," IEEE Trans. Magn. **45**, 1875–1918 (2009).

[23]S. Urazhdin, V. Tiberkevich, and A. Slavin, "Parametric excitation of a magnetic nanocontact by a microwave field," Phys. Rev. Lett. **105**, 237204 (2010).

[24]Z. M. Zeng, P. Upadhyaya, P. Khalili Amiri, K. H. Cheung, J. A. Katine, J. Langer, K. L. Wang, and H. W. Jiang, "Enhancement of microwave emission in magnetic tunnel junction oscillators through in-plane field orientation," Appl. Phys. Lett. **99**, 032503 (2011).

[25]T. Chen, A. Eklund, E. Iacocca, S. Rodriguez, B. G. Malm, J. Akerman, and A. Rusu, "Comprehensive and macrospin-based magnetic tunnel junction spin torque oscillator model—Part I: Analytical model of the MTJ STO," IEEE Trans. Electron Devices **62**, 1037–1051 (2015).

[26]P. K. Muduli, O. G. Heinonen, and J. Akerman, "Bias dependence of perpendicular spin torque and of free- and fixed-layer eigenmodes in MgO-based nanopillars," Phys. Rev. B **83**, 184410 (2011).

[27]A. N. Slavin and V. S. Tiberkevich, "Theory of mutual phase locking of spin-torque nanosized oscillators," Phys. Rev. B **74**, 104401 (2006).

[28]A. Houshang, R. Khymyn, H. Fulara, A. Gangwar, M. Haidar, S. R. Etesami, R. Ferreira, P. P. Freitas, M. Dvornik, R. K. Dumas, and J. Åkerman, "Spin transfer torque driven higher-order propagating spin waves in nano-contact magnetic tunnel junctions," Nat. Commun. **9**, 4374 (2018).

[29]A. Ruotolo, V. Cros, B. Georges, A. Dussaux, J. Grollier, C. Deranlot, R. Guillemet, K. Bouzehouane, S. Fusil, and A. Fert, "Phase-locking of magnetic vortices mediated by antivortices," Nat. Nanotechnol. **4**, 528–532 (2009).

[30]A. D. Belanovsky, N. Locatelli, P. N. Skirdkov, F. A. Araujo, J. Grollier, K. A. Zvezdin, V. Cros, and A. K. Zvezdin, "Phase locking dynamics of dipolarly

coupled vortex-based spin transfer oscillators," Phys. Rev. B **85**, 100409(R) (2012), 1202.5499.

[31]N. Locatelli, A. Hamadeh, F. Abreu Araujo, A. D. Belanovsky, P. N. Skirdkov, R. Lebrun, V. V. Naletov, K. A. Zvezdin, M. Muñoz, J. Grollier, O. Klein, V. Cros, and G. De Loubens, "Efficient synchronization of dipolarly coupled vortex-based spin transfer nano-oscillators," Sci. Rep. **5**, 17039 (2015).

[32]A. D. Belanovsky, N. Locatelli, P. N. Skirdkov, F. Abreu Araujo, K. A. Zvezdin, J. Grollier, V. Cros, and A. K. Zvezdin, "Numerical and analytical investigation of the synchronization of dipolarly coupled vortex spin-torque nano-oscillators," Appl. Phys. Lett. **103**, 122405 (2013).

[33]J. Persson, Y. Zhou, and J. Akerman, "Phase-locked spin torque oscillators: Impact of device variability and time delay," J. Appl. Phys. **101**, 09A503 (2007).

[34]J. Grollier, V. Cros, and A. Fert, "Synchronization of spin-transfer oscillators driven by stimulated microwave currents," Phys. Rev. B **73**, 060409(R).

[35]R. Lebrun, S. Tsunegi, P. Bortolotti, H. Kubota, A. S. Jenkins, M. Romera, K. Yakushiji, A. Fukushima, J. Grollier, S. Yuasa, and V. Cros, "Mutual synchronization of spin torque nano-oscillators through a long-range and tunable electrical coupling scheme," Nat. Commun. **8**, 15825 (2017).

[36]Y. Zhou, J. Persson, and J. Åkerman, "Intrinsic phase shift between a spin torque oscillator and an alternating current," J. Appl. Phys. **101**, 09A510 (2007).

[37]Y. Zhou, J. Persson, S. Bonetti, and J. Åkerman, "Tunable intrinsic phase of a spin torque oscillator," Appl. Phys. Lett. **92**, 092505 (2008).

[38]Y. Zhou and J. Åkerman, "Perpendicular spin torque promotes synchronization of magnetic tunnel junction based spin torque oscillators," Appl. Phys. Lett. **94**, 112503 (2009).

[39]V. Tiberkevich, A. Slavin, E. Bankowski, and G. Gerhart, "Phase-locking and frustration in an array of nonlinear spin-torque nano-oscillators," Appl. Phys. Lett. **95**, 262505 (2009).

[40]K. P. Kalinin and N. G. Berloff, "Complexity continuum within Ising formulation of NP problems," arXiv:2008.00466 (2020).

[41]V. Flovik, F. MacIà, and E. Wahlström, "Describing synchronization and topological excitations in arrays of magnetic spin torque oscillators through the Kuramoto model," Sci. Rep. **6**, 32528 (2016).

[42]T. Kanao, H. Suto, K. Mizushima, H. Goto, T. Tanamoto, and T. Nagasawa, "Reservoir computing on spin-torque oscillator array," Phys. Rev. Appl. **12**, 024052 (2019).